6-30-2016

A novel nano-energetic system based on bismuth hydroxide

Mkhitar A. Hobosyan
The University of Texas Rio Grande Valley

Srbuhi A. Yolchinyan
The University of Texas Rio Grande Valley

Karen S. Martirosyan
The University of Texas Rio Grande Valley

RSC Advances

PAPER

View Article Online
View Journal | View Issue

Cite this: *RSC Adv.*, 2016, **6**, 66564

A novel nano-energetic system based on bismuth hydroxide

Mkhitar A. Hobosyan, Srbuhi A. Yolchinyan and Karen S. Martirosyan*

Received 17th May 2016
Accepted 29th June 2016

DOI: 10.1039/c6ra12854h

www.rsc.org/advances

We report the first study of gas generation and thermal wave behavior during the performance of a novel nano-energetic system based on aluminum and bismuth hydroxide Al–$Bi(OH)_3$. Thermodynamic calculations demonstrate that this system is comparable to one of the most powerful known nano-thermite systems, Al–Bi_2O_3, in terms of energy capacity per initial charge mass, and may generate more than twice the gaseous products: 0.0087 mol g^{-1}. Differential scanning calorimetry analysis shows that homogenization of the as-received powder using mechanical activation is an essential step to reduce the decomposition energy of bismuth hydroxide by 30%. This results in nano-thermite with higher pressure discharge abilities. The mechanical activation with energy of 450–750 kJ g^{-1} is enough to transform micro-meter sized particles to sub-micro and nano-sized particles. The resulting nano-thermite generated a significant pressure discharge with a value of up to 5.6 kPa m^3 g^{-1}.

Introduction

Nano-thermites are energetic formulations of metallic fuel and oxidizer particles, where at least one constituent should be in the nano-size domain.[1–3] Oxidizers include traditional metal oxides such as Co_3O_4, Fe_2O_3, CuO and MoO_3, *etc.*,[4–7] as well as highly powerful nano-energetic gas generator (NGG) components such as iodine pentoxide I_2O_5 and bismuth trioxide Bi_2O_3.[8–14] Aluminum is one of the most popular metals utilized as a fuel, although Mg is also used occasionally.[15,16] Although much research has been performed to investigate the properties of metal oxide based nano-thermites,[17–22] other closely related systems based on metal hydroxides have surprisingly been overlooked. However, these systems undoubtedly deserve attention for several reasons. First of all, thermodynamic calculations (performed below) show that the energetic capacity per unit mass for Al–$Bi(OH)_3$ is close to that of Al–Bi_2O_3. This offers a strong indication that this system can generate sufficient pressure discharge and overtake almost all known nano-thermites. Furthermore, most of the methods for the production of bismuth trioxide particles utilize sol–gel methods, where the final product usually contains significant amounts of $Bi(OH)_3$ remnants. Thus, it is important to estimate the impact that these remnants can have on Al–Bi_2O_3 nano-thermite. Finally, we estimate that the Al–$Bi(OH)_3$ discharge generates twice the amount of gas per gram of initial thermite, when compared to gases generated in the Al–Bi_2O_3 system. Therefore, in applications where the utilization of gas generation with a lower average molecular weight is more important, then systems based on metal hydroxides can be superior to oxide based thermites. In this work, thermodynamic calculations, as well as pressure discharge dynamics, of the system Al–$Bi(OH)_3$ are investigated for the first time. Moreover, the effect of oxidizer particles size through high energy ball milling on the oxidizer decomposition and nano-thermite pressure discharge values are studied, and the milling energy and nano-thermite mass–pressure discharge dependences are revealed.

Thermodynamic analysis

Thermodynamic analysis of the Al–$Bi(OH)_3$ system is critical to evaluate the energetic capacity of the stoichiometric mixture, the adiabatic temperature, condensed phase concentrations and the amount of gaseous products released during the reaction. The thermodynamic estimation of the equilibrium composition of multicomponent multiphase systems requires minimization of the thermodynamic free energy (G), subject to mass and energy balances.[23] The thermodynamic calculations were made using "Thermo" software,[24] which includes a database containing the thermochemical properties of approximately 3000 compounds. We additionally used the thermochemical computer code HSC Chemistry-7 for the prediction of the adiabatic temperature and equilibrium compositions. Input and output species, as well as their amounts and initial temperatures, were defined for the calculations of adiabatic temperature and equilibrium concentrations. Theoretical heat balances were calculated by taking molecular amounts of the species from the reaction equations and equilibrium calculations. HSC Chemistry-7 includes a database of over 25 000 compounds.

Department of Physics, University of Texas at Rio Grande Valley, Brownsville, TX 78520, USA. E-mail: karen.martirosyan@utrgv.edu

The composition of the equilibrium products and adiabatic temperature can be determined by minimizing the thermodynamic potential. For a system with N(g) gas and N(s) solid number of components, at constant pressure, the concentrations of the equilibrium phases can be expressed as:

$$F(\{n_k\},\{n_s\}) = \sum_{k=1}^{N(g)} n_k\left(\ln\frac{p_k}{p} + G_k\right) + \sum_{l=1}^{N(s)} n_l G_l \quad (1)$$

where p_k is the partial pressure of the k-th gas-phase component, while n_l and G_l are the number of moles and molar Gibbs free energy of the components. The adiabatic combustion temperature, T_c^{ad}, is determined by the total energy balance:

$$\sum_{i=1}^{N_0} H_i(T_0) = \sum_{k=1}^{N(g)} n_k H_k\left(T_c^{ad}\right) + \sum_{l=1}^{N(s)} n_l H_l\left(T_c^{ad}\right) \quad (2)$$

where the enthalpy of each component is

$$H_i(T) = \Delta H_{f,i}^0 + \int_{T_0}^{T} c_{p,i}\mathrm{d}T + \sum \Delta H_{s,i} \quad (3)$$

and $\Delta H_{f,i}^0$ is the heat of formation at 1 atm and reference temperature T_0, $c_{p,i}$ is the heat capacity, and $\Delta H_{s,i}$ is the heat of s-th phase transition for the components.[25] The combination of both the above mentioned software programs made it possible to estimate the energetic capacity and predict the adiabatic interaction temperature and equilibrium product composition for the Al–$Bi(OH)_3$ system, which includes multiple phases at various temperatures. The interaction between Al and $Bi(OH)_3$ follows the reaction:

$$2Al + 2Bi(OH)_3 = Al_2O_3 + 2Bi + 3H_2O + \Delta H\ (-1.92\ kJ\ g^{-1}) \quad (4)$$

According to the HSC-7 calculations, the energetic capacity for the system (4) is 1.92 kJ g^{-1}, which is slightly less than the energetic capacity for the system Al–Bi_2O_3:

$$2Al + Bi_2O_3 = Al_2O_3 + 2Bi + \Delta H\ (-2.12\ kJ\ g^{-1}) \quad (5)$$

It is interesting to note that the energetic density calculated per unit volume for the system (4) is 8.83 kJ cm^{-3}, while the energetic density for the system (5) is 15.2 kJ cm^{-3}. Fig. 1 shows the dependence of the adiabatic temperature and equilibrium concentration of the condensed and gaseous phases during the exothermic reaction in system (4). System (5) appears to have a higher energetic capacity per mass and per volume. However, if we assume that due to high temperatures of about 3000 K, only the Bi particles (boiling point at 1832 K (ref. 26)) and water will transform into the gaseous phase (the Al_2O_3 boiling point is 3250 K (ref. 27)), then the gaseous products generated for system (5) per unit mass of the initial mixture is 0.00385 mol g^{-1}, while system (4) generates twice this, at the higher amount of 0.0087 mol g^{-1}. This can be a very important advantage of hydroxide systems over oxide type thermites for applications where a high amount of gaseous products per initial charge mass is vital, such as micro-propulsions and micro-thrusters for space applications.[28–30] When the molar ratio Al/$Bi(OH)_3$ increases from 0.5 to 1, the system follows eqn (4). However, when the ratio increases above 1, the temperature increases to more than 2000 K, resulting in the gradual decomposition of water into hydrogen, and the released oxygen is consumed for excess aluminum oxidation. At a molar ratio of 2, the highest adiabatic temperature is calculated to be 2970 K, where the products are about 1 mol solid Al_2O_3, 1 mol gaseous Bi, and ~1.6 mol of a gaseous mixture of molecular H_2 and atomic hydrogen. At this point, the reaction pathway becomes

$$2Al + Bi(OH)_3 = Al_2O_3 + Bi(g) + 1.4H_2(g) + 0.2H(g) \quad (6)$$

The further increase in the fuel to oxidizer molar ratio results in some partial decomposition of solid Al_2O_3 into gaseous Al_2O and gaseous Al. However the amount of atomic hydrogen quickly decreases due to the reduction in adiabatic temperature. Thus, in our experiments we used a molar ratio for Al and bismuth hydroxide of 2 according to reaction (6). We also took into account the extra oxide shell mass on the aluminum nanoparticles. In addition, we investigated the pressure discharge dependence on the non-stoichiometric fuel to oxidizer ratio, for comparison with the thermodynamic calculations.

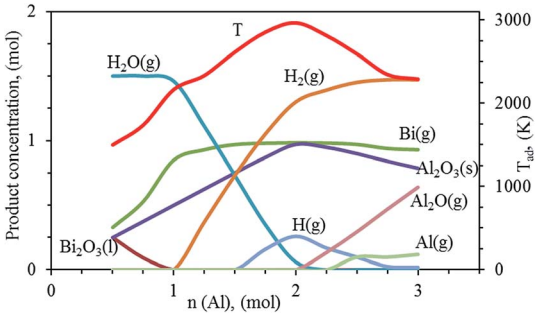

Fig. 1 Dependence of the adiabatic temperature and equilibrium concentration of condensed and gaseous phases on the fuel concentration during the exothermic reaction in the Al–$Bi(OH)_3$: system (red line is adiabatic combustion temperature).

Experimental methods and procedures

The aluminum nanoparticles with an average particle size of 100 nm (87%, covered with 13% Al_2O_3) used for nano-thermite preparation were purchased from Sigma Aldrich Co and stored under nitrogen (99.98%) to avoid any contamination and oxidation. Bismuth hydroxide (99%) was purchased from Acros Organics. Bismuth trioxide, Bi_2O_3, was purchased from Sigma Aldrich (99.9%, 10 μm).

The $Bi(OH)_3$ particles were milled in a High Energy Ball Mill (HSF-3, MTI Co) machine for up to 15 min. In the milling media, the ball to powder weight ratio was 10 : 1. The powder batch mass was 0.01 kg. We homogenized the $Bi(OH)_3$ using high-energy ball milling for up to 15 min with 5 min time increments, to control the effect of the mechanical activation on the particle size reduction, decomposition energy of bismuth hydroxide, and oxidizing activity in the Al–$Bi(OH)_3$ nanostructured system.

The milling energy applied during the mechanical activation decreases the particle size of the bismuth hydroxide particles. We calculated the energy dose transferred to the powder batch using the method described in ref. 31. The effects of the milling time and treatment energy of the Al–$Bi(OH)_3$ system on the pressurization rate were determined.

Al–$Bi(OH)_3$ nano-thermite formulations were prepared with various mass ratios, which are fuel rich to compensate for the presence of the aluminum oxide shell on the metal nanoparticles. While the stoichiometric mass ratio was 1.1 : 8.9, a ratio of 2 : 8 was found experimentally as the best ratio to obtain the highest pressure discharge value.

The thermite was mixed using a roller ball mill in an alumina jar with zirconia balls (5 mm in diameter) under a hexane environment for 9 h, and was then dried under vacuum for 12 h. The resulting nano-thermite powder was placed into a cylindrical charge holder with a volume of 0.4 cm^3 (the bulk density was ~0.6 g cm^{-3}) for the charge of 0.2 g mass (for another set of experiments, the mass was increased up to 0.5 g to observe pressure discharge dependence on nano-thermite mass). The holder was placed into a Parr Instrument High Pressure Cylindrical Reactor with a volume of 0.342 L. The detonation was electrically triggered using a Ni–Cr micro-wire, the pressure signals were received by a piezoelectric transducer with rated pressure/voltage values (omega) and the signals were amplified and recorded through an omega DAQ-3005 Data Acquisition board with a signal acquisition frequency of 1 MHz.

Thermo-gravimetric analysis (TGA) was performed using a Differential Scanning Calorimeter (DSC) with a sensitivity of 0.1 μg (Q-600, TA Instruments). The measurements were made under a nitrogen atmosphere (99.98% purity).

A Nicolet iS5 FTIR spectrometer (Thermo Scientific) with an ID-5 accessory was used to perform Fourier Transform Infrared (FTIR) spectroscopy on a small quantity (~5 mg) of powder that was pressed to obtain a flat surface. The measurement was performed in the wavenumber range of 4000–400 cm^{-1}.

XRD analysis was performed using a Bruker D-2 Phaser with a Cu K_α anode, in the 2θ range of 20–60, where the main peaks of bismuth hydroxide and oxide are distributed. The scans were taken with a θ precision of 0.02° and the sample was rotated at 15 rpm to statistically increase the number of particles contributing to the XRD signal intensity. To avoid statistical variation in the experimental parameters such as the amount of powder, surface flatness and number of particles in preferred directions, *etc.*, the peak intensities are given with relative intensity values, represented as a ratio between the intensity of the peaks to the intensity of the highest peak for each sample.

Particle morphology, composition and size distribution analyses were performed using a JEOL 7800F Field Emission Scanning Electron Microscope, equipped with an Electron Dispersive X-ray Spectroscopy system (EX-37270VUP).

Results and discussion

Bismuth hydroxide particle characterization

Thermo-gravimetric analysis and differential scanning calorimetry of the as-received and mechanically activated bismuth hydroxide powders are essential to estimate the amount of absorbed humidity and observe the decomposition characteristics of the oxidizer, $Bi(OH)_3$. We expect that upon heating, bismuth hydroxide decomposes into bismuth oxide according to the following simplified reaction pathway:

$$2Bi(OH)_3(s) \rightarrow Bi_2O_3(s) + 3H_2O(g) \text{ (mass reduction 10.4 wt\%)} \quad (7)$$

The decomposition of bismuth hydroxide is complicated and includes several steps. Fig. 2a represents the heat flow and weight change dependence on temperature for the as received $Bi(OH)_3$ powder. The blue line represents the weight change (wt%), the green line shows the heat flow (W g^{-1}), and the red line indicates the points through which the heat flow peaks are integrated to estimate the energy required for decomposition (J g^{-1}). The DSC was pre-calibrated for heat flow curve integration. The decomposition of bismuth hydroxide starts at around 390 °C with a degradation energy of 28.8 J g^{-1}. The second mass loss starts immediately at around 502 °C with a corresponding decomposition energy of 78.5 J g^{-1} for the last step. The decomposition is essentially complete at around 590 °C. The energy required for all steps of the decomposition process is around 107 J g^{-1}. Beyond 600 °C, no weight loss or thermal effect is recorded until 700 °C is reached, where only the pure Bi_2O_3 phase is present. The overall mass loss is about 9.7 wt%, close to the theoretical estimation from eqn (7). Thus, the as-received powder contains a very small amount of Bi_2O_3 (the XRD measurements below confirm the presence of trace amounts of Bi_2O_3).

Milling bismuth hydroxide for up to 10 min results in 3-step mass loss and significantly reduces the energy required for complete decomposition. Fig. 2b presents the DSC results for $Bi(OH)_3$ treated for 10 min in a high energy ball mill. The weight loss starts at around 395 °C with an energy consumption of 25.1 J g^{-1} for the first step and a significant energy decrease from 78.5 J g^{-1} to 50.4 J g^{-1} is then observed for the second step, resulting in a new endotherm with an energy of 6.5 J g^{-1} at the end. This might be due to increased defects in the crystal structure, and the weight loss is also stretched and delayed in this case. Thus, the energy required for the complete decomposition is about 82 J g^{-1}, *i.e.* 23% less than that for the as-received $Bi(OH)_3$. Apparently, the milling not only reduces the particle size to the sub-micrometer domain (see particle morphology characterization below), but also creates multiple defects in the crystallographic structure, thus reducing the decomposition energy.

Further milling of the particles does not bring significant changes to the overall decomposition energy. For the particles milled for 15 min, the first step consumes 23.8 J g^{-1} of energy, the second endotherm decreases to an energy of 41.5 J g^{-1} (Fig. 2c) and the energy for the last step increases to 11 J g^{-1}. The overall decomposition energy is about 76 J g^{-1}, which is 29% less than that for the as-received powder. The comparison of the decomposition energies is especially important, because in nano-thermite a fraction of the energy released from Al–$Bi(OH)_3$ will be consumed by the oxidizer particle

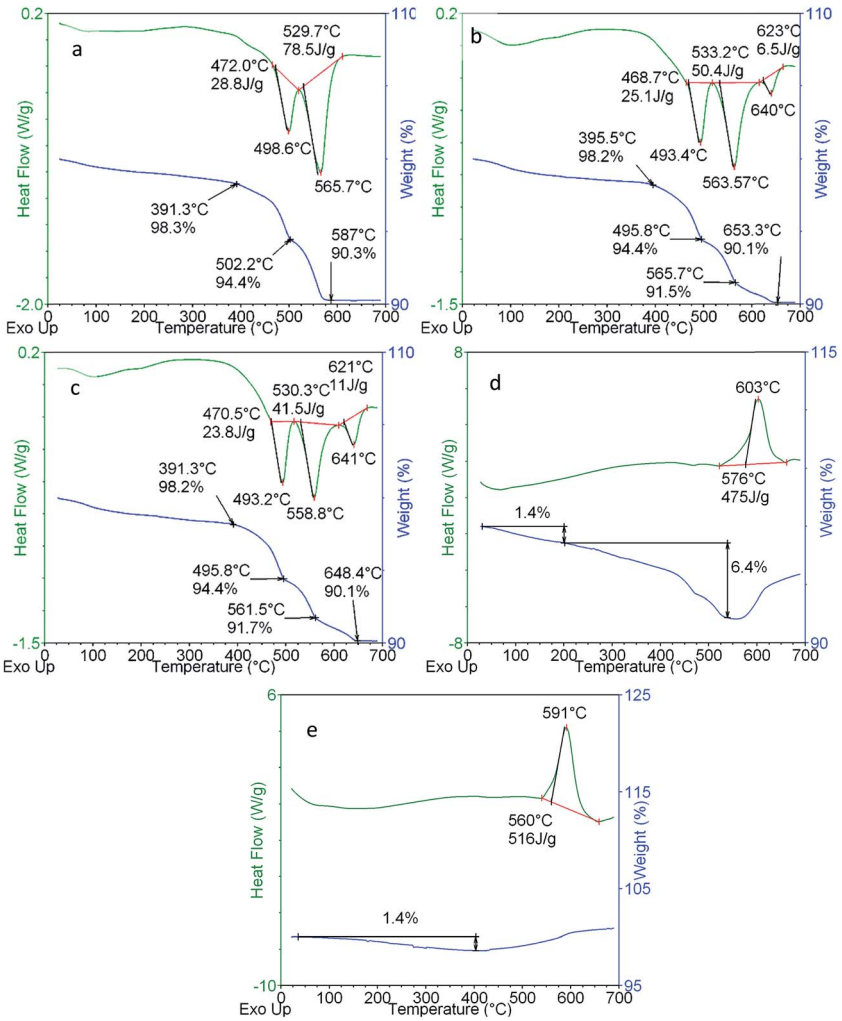

Fig. 2 Heat flow and weight change dependence on the temperature for: (a) as received $Bi(OH)_3$; (b) 10 min milled $Bi(OH)_3$; (c) 15 min milled $Bi(OH)_3$; (d) Al–$Bi(OH)_3$ mixture; (e) Al–Bi_2O_3 mixture.

decomposition. Thus, a lower decomposition energy of the oxidizer is beneficial for the nano-thermite pressure discharge ability. Therefore, we expect that a 15 min treatment of $Bi(OH)_3$ should give thermite an increased discharge energy. Further milling of bismuth hydroxide particles does not reduce the overall decomposition energy as presented in Fig. 3, thus for further experiments $Bi(OH)_3$ particles milled for up to 15 min were used.

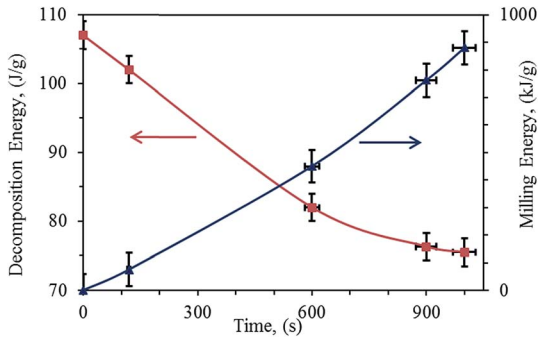

Fig. 3 The decomposition energy and milling energy dependence on the milling time for the $Bi(OH)_3$ particles.

To compare the heat released in the systems Al–$Bi(OH)_3$ and Al–Bi_2O_3, we performed DSC analysis of these systems (Fig. 2d and e). Both mixtures were prepared under the same conditions (9 h mixing in hexane). The Al–$Bi(OH)_3$ system shows a 475 J g^{-1} energy release at around 576 °C (Fig. 2d), which is about 8% less than the exothermic peak in the Al–Bi_2O_3 system at around 560 °C (516 J g^{-1}, Fig. 2e). We should mention that before the vigorous exothermic reaction, the Al–$Bi(OH)_3$ composition experienced a stepwise weight loss of about 7.8 wt%, as due to the slow heating rate (20 °C min^{-1}), the OH groups partially escaped.

It is important to note, that Al–$Bi(OH)_3$ is practically stable up to 200 °C, losing only about 1.4 wt% due to the evaporation of residual solvents and absorbed moisture. However, at temperatures above 200 °C, we see gradual mass reduction up to the ignition point of nano-thermite at 550 °C.

The XRD measurements for the as-received particles and the powder milled for 15 min are presented in Fig. 4a. The initial

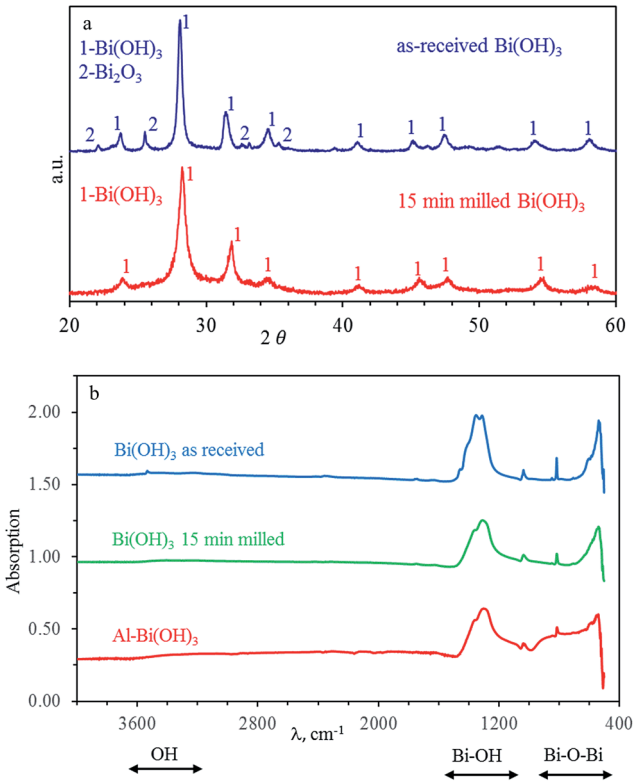

Fig. 4 (a) XRD patterns for as-received $Bi(OH)_3$ and 15 min milled $Bi(OH)_3$, (b) FTIR absorption for as-received $Bi(OH)_3$, 15 min milled $Bi(OH)_3$, and Al–$Bi(OH)_3$ prepared mixture using 15 min milled $Bi(OH)_3$.

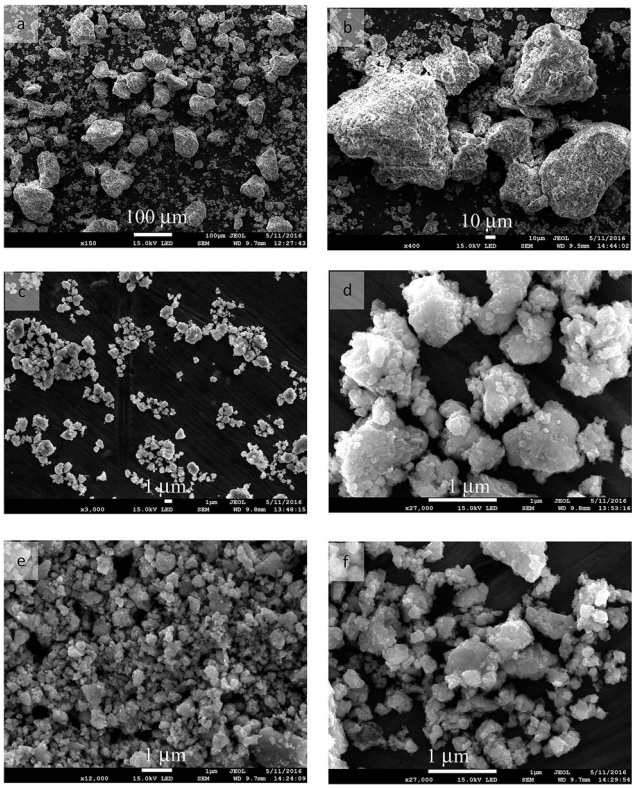

Fig. 5 SEM images for (a, b) as received $Bi(OH)_3$; (c, d) 10 min milled $Bi(OH)_3$; (e, f) 15 min milled $Bi(OH)_3$.

powder has sharper peaks, due to coarser particles with sizes of up to 100 μm (see SEM characterization below). The crystallite size was estimated to be 270 Å, using Sherrer's formula.[11] The milling of the particles reduces the average particle size to the sub-micrometer and nano-size domain, and the crystallite size is reduced to 170 Å, and as a result broader peaks appear (15 min milled particles). The traces of bismuth oxide also disappear in the process of homogenization through the milling processes.

Fig. 4b presents the FTIR measurements for the as-received particles of $Bi(OH)_3$, the $Bi(OH)_3$ particles milled for 15 min, and the nano-energetic mixture Al–$Bi(OH)_3$. The absorption peaks at 600–800 cm^{-1} correspond to Bi–O–Bi bonds, while the peaks at 1100–1400 cm^{-1} correspond to Bi–OH groups.[32] The reaction product did not exhibit significant absorption in the IR region.

The particle size and morphology observations using SEM show that the as-received particles are coarse with particle sizes of up to 100 μm, as shown in Fig. 5a and b. Milling for 10 min critically reduces the portion of micrometer-sized particles and produces mostly those of sub-micrometer size, as well as nanometer sized particles, as shown in Fig. 5c and d. The increased milling time of up to 15 min results in a higher amount of submicron and nano-meter sized particles (Fig. 5e and f). Further increasing the milling time beyond 15 min does not result in a significant reduction in particle size.

The SEM image of nano-thermite Al with bismuth hydroxide (milled for 15 min) is presented in Fig. 6a. The small (~100 nm) Al nanoparticles are well distributed in the sub-micrometer sized $Bi(OH)_3$ media. The image of higher magnification shows individual Al nanoparticles surrounding $Bi(OH)_3$ particles (Fig. 6b). The EDS mapping of elemental Al and Bi for

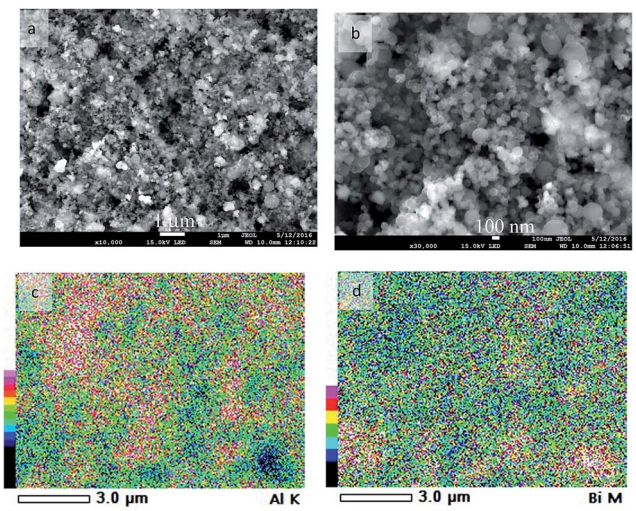

Fig. 6 (a, b) SEM images of Al–$Bi(OH)_3$ (15 min milled) nano-thermite, bar length 1 μm and 100 nm, respectively; (c, d) EDX mapping for Al and Bi elements for the region shown in (a).

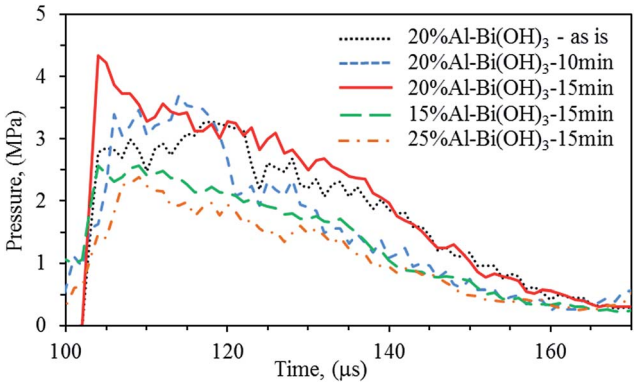

Fig. 7 Discharge pressure dependence on time for Al–$Bi(OH)_3$ thermites prepared with as received, 10 and 15 min mechanical treated $Bi(OH)_3$, with 20 wt% Al, and thermite prepared with 15 min treated $Bi(OH)_3$ and different weight percentages of Al.

the same area shown in Fig. 6a is presented in Fig. 6c and d, respectively. The bar on the left side of the maps represents the relative concentration of each element. The distribution of Al and Bi atoms is consistent with the corresponding particle locations.

Pressure discharge

Al–$Bi(OH)_3$ thermite was prepared using Al nanopowder with an average particle size of 100 nm and bismuth hydroxide (as received, and milled for 10 or 15 min) at various fuel to oxidizer ratios. Fig. 7 presents the pressure *vs.* time plot for Al–$Bi(OH)_3$ thermites prepared with the as received and treated $Bi(OH)_3$ powder for up to 10 or 15 min with different weight percentages of Al. The highest pressure obtained for the thermite prepared with the as-received $Bi(OH)_3$ was 3.33 MPa for 0.2 g thermite, while the value for the $Bi(OH)_3$ treated for 10 min was 3.71 MPa (11% pressure rise) and that for the $Bi(OH)_3$ treated for 15 min was 4.34 MPa (30% pressure rise). For all cases the pressure fluctuates near the peak value for about 20 microseconds. The nano-thermites prepared with bismuth hydroxide that were milled for a longer time (up to 20 min) exhibit identical performance to the powder milled for 15 min. The 20 wt% Al and 80 wt% $Bi(OH)_3$ thermite generates the highest pressure of 4.34 MPa compared to 2.67 MPa for 15 wt% Al and 2.41 MPa for 25 wt% Al containing thermites, for a 0.2 g nano-thermite charge mass.

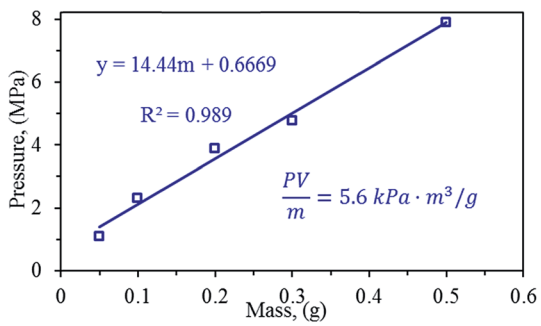

Fig. 8 The pressure dependence on thermite weight for Al–$Bi(OH)_3$ nano-thermite.

Fig. 8 presents the pressure discharge dependence on the nano-thermite loading charge mass. This thermite was prepared *via* a conventional roller mixing method, using the 15 min treated $Bi(OH)_3$ and 20 wt% Al in a hexane environment with a mixing time of up to 9 h. The specific multiplication factor for this thermite was $\sim 14.44m + 0.6669$ (*i.e.* a 1 g loading charge would generate a 15.1 MPa pressure in a volume of 0.342 L). The pressure × volume (PV) value for this powder per mass was 5.6 kPa m^3 g^{-1}, which is comparable to one of the highest values reported in the nano-energetic literature.[2]

Conclusions

Al–$Bi(OH)_3$ is a novel and powerful nano-energetic system with pressure discharge values comparable to one of the most powerful systems, Al–Bi_2O_3. According to thermodynamic calculations, this mixture exhibits twice the gas generation abilities when the fuel to oxidizer stoichiometric molar ratio is near 2 : 1, compared to the Al–Bi_2O_3 system, which is important for applications that require high amounts of gaseous products such as micro-thrusters. The homogenization of the bismuth hydroxide micro-sized particles in a high energy ball mill for 15 min converts the particles to the sub-micrometer and nano-sized domain, and reduces the decomposition energy by about 30%. The resulting bismuth hydroxide powder is highly reactive, and mixing with aluminum forms nano-thermite generating pressure × volume values of up to 5.6 kPa m^3 g^{-1}. The best mass ratio for generating the highest pressure discharge value is 2 : 8 fuel to oxidizer. Metal hydroxides are promising components for nano-thermites, which may generate a vigorous amount of gaseous products and have extreme pressure discharge abilities.

Acknowledgements

We would like to acknowledge the financial support for this research in part from the Army Research Office (grant No. 66389-CH-REP) and NSF PREM (award DMR-1523577: UTRGV-UMN Partnership for Fostering Innovation by Bridging Excellence in Research and Student Success).

References

1 D. D. Dlott, Thinking big (and small) about energetic materials, *Mater. Sci. Technol.*, 2006, **22**(4), 463–473.
2 K. S. Martirosyan, Nanoenergetic gas generators, principle and applications, *J. Mater. Chem.*, 2011, **21**, 9400–9405.
3 S. Kyle and M. Zachariah, Simultaneous pressure and optical measurements of nanoaluminum thermites: investigating the reaction mechanism, *J. Propul. Power*, 2010, **26**(3), 467–472.
4 V. K. Patel, J. Raj Saurav, K. Gangopadhyay, S. Gangopadhyay and S. Bhattacharya, Combustion characterization and modeling of novel nanoenergetic composites of Co_3O_4/*n*Al, *RSC Adv.*, 2015, **5**(28), 21471–21479.

5 J. L. Cheng, H. H. Hng, H. Y. Ng, P. C. Soon and Y. W. Lee, Synthesis and characterization of self-assembled nanoenergetic Al–Fe_2O_3 thermite system, *J. Phys. Chem. Solids*, 2010, **71**(2), 90–94.

6 S. Demitrios, Z. Jiang, V. K. Hoffmann, M. Schoenitz and E. L. Dreizin, Fully dense, aluminum-rich Al–CuO nanocomposite powders for energetic formulations, *Combust. Sci. Technol.*, 2008, **181**(1), 97–116.

7 S. M. Umbrajkar, M. Schoenitz and E. L. Dreizin, Control of Structural Refinement and Composition in Al–MoO_3 Nanocomposites Prepared by Arrested Reactive Milling, *Propellants, Explos., Pyrotech.*, 2006, **31**(5), 382–389.

8 K. S. Martirosyan, L. Wang and D. Luss, Novel nanoenergetic system based on iodine pentoxide, *Chem. Phys. Lett.*, 2009, **483**(1), 107–110.

9 B. R. Clark and M. L. Pantoya, The aluminium and iodine pentoxide reaction for the destruction of spore forming bacteria, *Phys. Chem. Chem. Phys.*, 2010, **12**(39), 12653–12657.

10 M. Hobosyan, A. Kazansky, and K. S. Martirosyan, Nanoenergetic composite based on I_2O_5/Al for biological agent defeat, in *Technical Proceeding of the 2012 NSTI Nanotechnology Conference and Expo*, 2012, pp. 599–602.

11 K. S. Martirosyan, L. Wang, A. Vicent and D. Luss, Synthesis and performance of bismuth trioxide nanoparticles for high energy gas generator use, *Nanotechnology*, 2009, **20**(40), 405609.

12 V. K. Patel, A. Ganguli, R. Kant and S. Bhattacharya, Micropatterning of nanoenergetic films of Bi_2O_3/Al for pyrotechnics, *RSC Adv.*, 2015, **5**(20), 14967–14973.

13 J. A. Puszynski, C. J. Bulian and J. J. Swiatkiewicz, Processing and ignition characteristics of aluminum–bismuth trioxide nanothermite system, *J. Propul. Power*, 2007, **23**(4), 698–706.

14 L. Wang, D. Luss and K. S. Martirosyan, The behavior of nanothermite reaction based on Bi_2O_3/Al, *J. Appl. Phys.*, 2011, **110**(7), 074311.

15 W. Haiyang, G. Jian, G. C. Egan and M. R. Zachariah, Assembly and reactive properties of Al/CuO based nanothermite microparticles, *Combust. Flame*, 2014, **161**(8), 2203–2208.

16 X. Zhou, D. Xu, G. Yang, Q. Zhang, J. Shen, J. Lu and K. Zhang, Highly exothermic and superhydrophobic Mg/fluorocarbon core/shell nanoenergetic arrays, *ACS Appl. Mater. Interfaces*, 2014, **6**(13), 10497–10505.

17 N. W. Piekiel, L. Zhou, K. T. Sullivan, S. Chowdhury, G. C. Egan and M. R. Zachariah, Initiation and Reaction in Al/Bi_2O_3 Nanothermites: Evidence for the Predominance of Condensed Phase Chemistry, *Combust. Sci. Technol.*, 2014, **186**(9), 1209–1224.

18 R. R. Nellums, B. C. Terry, B. C. Tappan, S. F. Son and L. J. Groven, Effect of Solids Loading on Resonant Mixed Al–Bi_2O_3 Nanothermite Powders, *Propellants, Explos., Pyrotech.*, 2013, **38**(5), 605–610.

19 M. Kevin, M. L. Pantoya and S. F. Son, Combustion behaviors resulting from bimodal aluminum size distributions in thermites, *J. Propul. Power*, 2007, **23**(1), 181–185.

20 X. Zhou, M. Torabi, J. Lu, R. Shen and K. Zhang, Nanostructured energetic composites: synthesis, ignition/combustion modeling, and applications, *ACS Appl. Mater. Interfaces*, 2014, **6**(5), 3058–3074.

21 V. Baijot, L. Glavier, J.-M. Ducéré, M. Djafari Rouhani, C. Rossi and A. Estève, Modeling the Pressure Generation in Aluminum-Based Thermites, *Propellants, Explos., Pyrotech.*, 2015, **40**(3), 402–412.

22 Qi-L. Yan, M. Gozin, F.-Q. Zhao, A. Cohen and Si-P. Pang, Highly energetic compositions based on functionalized carbon nanomaterials, *Nanoscale*, 2016, **8**(9), 4799–4851.

23 W. Greiner, L. Neise and H. Stöcker, *Thermodynamics and statistical mechanics*, Springer-Verlag, 1995, vol. 101.

24 A. A. Shiryaev, Thermodynamics of SHS Processes: Advanced Approach, *Int. J. Self-Propag. High-Temp. Synth.*, 1995, **4**(4), 351–362.

25 V. Arvind, A. S. Rogachev, A. S. Mukasyan and S. Hwang, Combustion synthesis of advanced materials: principles and applications, *Adv. Chem. Eng.*, 1998, **24**, 79–226.

26 J. A. Cahill and A. D. Kirshenbaum, The density of liquid bismuth from its melting point to its normal boiling point and an estimate of its critical constants, *J. Inorg. Nucl. Chem.*, 1963, **25**(5), 501–506.

27 R. C. Rowe, P. J. Sheskey, and M. E. Quinn, *Handbook of pharmaceutical excipients*, Pharmaceutical Press, 2009, pp. 11–12.

28 K. S. Martirosyan, M. Hobosyan and S. E. Lyshevski, Enabling nanoenergetic materials with integrated microelectronics and MEMS platforms, in *Nanotechnology (IEEE-NANO), 2012 12th IEEE Conference on*, IEEE, 2012, pp. 1–5.

29 I. Puchades, M. Hobosyan, L. F. Fuller, F. Liu, S. Thakur, K. S. Martirosyan, and S. E. Lyshevski, MEMS microthrusters with nanoenergetic solid propellants, in *Nanotechnology (IEEE-NANO), 2014 IEEE 14th International Conference on*, IEEE, 2014, pp. 83–86.

30 C. Rossi, K. Zhang, D. Esteve, P. Alphonse, P. Tailhades and C. Vahlas, Nanoenergetic materials for MEMS: a review, IEEE/ASME, *J. Microelectromech. Syst.*, 2007, **16**(4), 919–931.

31 F. Delogu and C. Deidda, A quantitative approach to mechanochemical processes, *J. Mater. Sci.*, 2004, **39**, 5121–5124.

32 E. Bartonickova, J. Cihlar and K. Castkova, Microwave-assisted synthesis of bismuth oxide, *Process. Appl. Ceram.*, 2007, **1**(1), 29–33.

